JOURNAL OF SPACECRAFT AND ROCKETS
Vol. 40, No. 5, September–October 2003

Computational Fluid Dynamics Prediction of the Beagle 2 Aerodynamic Database

Peter A. Liever* and Sami D. Habchi†
CFD Research Corporation, Huntsville, Alabama 35805
and
Simon I. Burnell‡ and J. Steve Lingard§
Martin–Baker Aircraft, Ltd., Higher Denham, England UB9 5AJ, United Kingdom

Flowfield solutions over the Beagle 2 Mars probe aeroshell, spanning the trajectory through the Martian atmosphere, have been generated for the continuum flow regime for Mach numbers from 1.5 to 28 at angles of attack from 0 to 11 deg. Static aerodynamic coefficients C_A, C_N, and C_m were derived from flow solutions generated by computational fluid dynamics (CFD) analysis. CFD derived data were applied, together with scaled existing data and wind tunnel experiments, to develop a static aerodynamic database applied in the entry and descent predictions for the Beagle 2 development program.

Nomenclature

A	=	projected area, m^2
C_A	=	axial force coefficient
C_m	=	pitching moment coefficient
C_N	=	normal force coefficient
C_p	=	pressure coefficient
$C_{p\,\max}$	=	normal shock stagnation point pressure coefficient
D	=	vehicle diameter, m
Kn	=	Knudsen number
M	=	Mach number
P	=	pressure, N/m^2
Q	=	freestream dynamic pressure, N/m^2
T	=	temperature, K
U	=	freestream velocity, m/s
α	=	angle of attack, deg
γ	=	ratio of specific heats
θ	=	local flow impact angle, deg
ρ	=	density, kg/m^3

Introduction

BEAGLE 2 is a British-led project to land a probe on Mars as part of the ESA's Mars Express Mission to be launched in June 2003. The geometry is based on the Huygens probe, with the major difference being the addition of a backshell frustrum enclosing the payload.

Martin–Baker Aircraft, Ltd., has been tasked with the overall responsibility for the Beagle 2 entry vehicle design. The entry, descent, and landing (EDL) system has been designed to eject the Beagle 2 safely from the Mars Express orbiter and deliver a 30-kg scientific payload to the surface of Mars. To achieve this objective, Martin–Baker Aircraft, Ltd., adopted the following design approach: 1) ballistic entry, 2) a high drag shape with good static stability characteristics, and 3) a simple generic shape to take maximum advantage of existing aerodynamic data and to simplify analysis. These first three constraints led to the selection of an axisymmetric shape, specifically a large-angle sphere cone: 4) nose radius selected for minimum structural mass with maximum drag, leading to a maximized radius limited by the range of bluntness ratios in existing aerodynamic databases and heating requirements; 5) corner radii minimized for maximum drag, limited by structural/thermal requirements; and 6) interpolation within existing data where possible, rather than extrapolation. This may lead to suboptimal design, but higher confidence.

Constraints on cost and time, due to launch opportunity and mission length, made it necessary to generate a static database quickly by the reuse of existing data. A continuum-based static aerodynamic coefficient database was generated with density-based Navier–Stokes codes with the appropriate thermochemical models. Computed aerodynamic data were then used to scale available databases of geometrically similar vehicles to develop an aerodynamic database for the Beagle 2. CFD Research Corp.'s (CFDRC's) CFD-FASTRAN code[1] and Fluid Gravity's TINA code[2] were employed in computational fluid dynamics (CFD) predictions of flowfield, aerodynamic, and heating characteristics of the Beagle 2. This paper reports on CFDRC's efforts in computing the continuum aerodynamic coefficient database.

Beagle 2 Geometry

The Beagle 2 forebody design is geometrically similar to the Huygens entry vehicle forebody design, which maximizes data reuse from the Huygens program. Unlike Huygens, however, Beagle 2 geometry incorporates a continuous rear cover design, with a small backward-facing step at the junction between the backcover and front shield to ensure a consistent separation point (Fig. 1). This reduces the risk of the separated shear layer impinging on the backshell, and reduces the size of the recirculation region, which, in turn, minimizes the risk of asymmetries in the base flow.

The forebody of the Beagle 2 aeroshell is a 60-deg half-angle cone with a maximum vehicle diameter $D = 0.9$ m. It has a spherically blunted nose of radius 0.417 m and a shoulder radius of 0.029 m (Fig. 2). (Huygens maximum vehicle diameter and nose radius were 2.7 and 1.25 m, respectively.) The corner radius for Beagle 2 has been chosen to match the peak heat transfer at this point with the peak stagnation point heat transfer, thus allowing a constant thermal protection thickness. The mass of the Beagle 2 EDL system, together with the lander, is approximately 60 kg.

The backshell of Beagle 2 is inclined by approximately 47 deg relative to the vehicle's axis of symmetry. A minimum for this angle was based on the need to avoid shear-layer impingement and from the availability of published aerodynamic data. A flat base cover

Presented as Paper 2002-0683 at the AIAA 40th Aerospace Sciences Meeting, Reno, NV, 14–17 January 2002; received 18 March 2002; revision received 12 June 2002; accepted for publication 17 February 2003. Copyright © 2003 by the authors. Published by the American Institute of Aeronautics and Astronautics, Inc., with permission. Copies of this paper may be made for personal or internal use, on condition that the copier pay the $10.00 per-copy fee to the Copyright Clearance Center, Inc., 222 Rosewood Drive, Danvers, MA 01923; include the code 0022-4650/03 $10.00 in correspondence with the CCC.

*Principal Engineer, Aeromechanics Branch. Senior Member AIAA.
†Director, Aeromechanics Branch. Senior Member AIAA.
‡Senior Systems Engineer, Space Systems Division. Member AIAA.
§Chief Systems Engineer, Space Systems Division. Member AIAA.

Fig. 1 Beagle 2 aeroshell configuration.

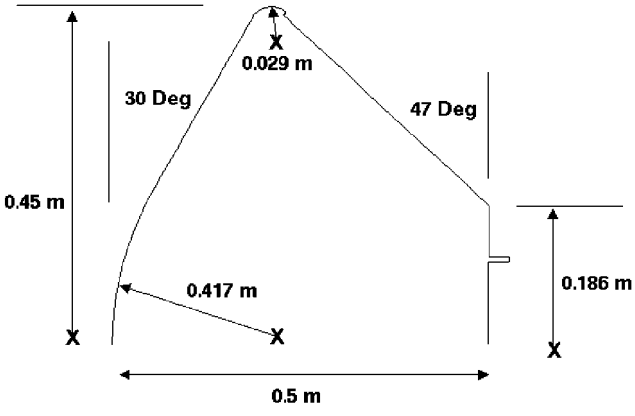

Fig. 2 Geometric dimensions of Beagle 2.

was chosen with a sharp transition from the rear cone. Various protrusions and excrescencies on the vehicle base, such as the launch clamp ring and connectors, were not modeled during the derivation of the static aerodynamic coefficients. However, the effect of the launch clamp ring was analyzed separately and is discussed later.

Trajectory-Derived Aerodynamic Database Matrix

A six-degree-of-freedom (6-DOF) trajectory code developed at Martin–Baker Aircraft, Ltd. was used to perform both Monte Carlo simulations and a sensitivity analysis. The simulation includes a Martian atmosphere model (NASA MarsGRAM[3]), a wind model, and a gravity model. Based on a dispersion analysis about the nominal entry conditions, the entry flight-path angle for Beagle 2 has been calculated to lie within the range from −21 to −15 deg at an altitude of 120 km above the planet surface. The nominal trajectory shown in Fig. 3, used in the derivation of the aerodynamic database, is based on an entry flight-path angle of −18 deg.

Nine trajectory points, listed in Table 1, for Mach numbers ranging from 1.5 to 28, were extracted along the nominal trajectory. Aerodynamic coefficients were computed for a matrix of 37 flight conditions for the nine trajectory points and angles of attack from 0 to 11 deg. Analyses were performed at angles of attack up to 5 deg for the entire regime. Angles up to 11 deg were analyzed for the transonic/supersonic lower end of the spectrum and for the high Mach number, high-altitude upper end. (Blunt entry vehicles are known to experience reduced pitch stability at those conditions, possibly resulting in larger angles of attack.) The resulting solution matrix is shown in Table 2.

Computational Model

CFD-FASTRAN Flow Solver

CFDRC's CFD-FASTRAN[1] program was used to compute the Beagle 2 flowfield and determine the resulting aerodynamic forces. CFD-FASTRAN is a compressible finite volume flow solver for thermochemical nonequilibrium flow analysis. Structured grids

Table 1 Beagle 2 nominal trajectory points

Mach number	Velocity, m/s	Temperature, K	Pressure, Pa
28	5386	156.8	1.4
25	5061	170.8	8.9
20	4248	184.5	29.1
15	3256	191.1	59.3
10	2200	195.6	104.0
7	1552	198.3	144.9
5	1117	200.6	185.7
3	677	204.3	257.7
1.5	345	209.2	398.3

Table 2 Solution matrix for Beagle 2 aerodynamic database

	α, deg					
M	0	2	5	8	11	Gas chemistry
28	—	•	•	•	•	Reacting
25	—	•	•	•	•	Reacting
20	•	•	•	•	•	Reacting
15	—	•	•	•	—	Reacting
10	—	•	•	•	—	Reacting
7	•	•	•	—	—	Reacting
7	•	•	•	—	—	Nonreacting
5	—	•	•	—	—	Nonreacting
3	•	•	•	•	•	Nonreacting
1.5	•	•	•	•	•	Nonreacting

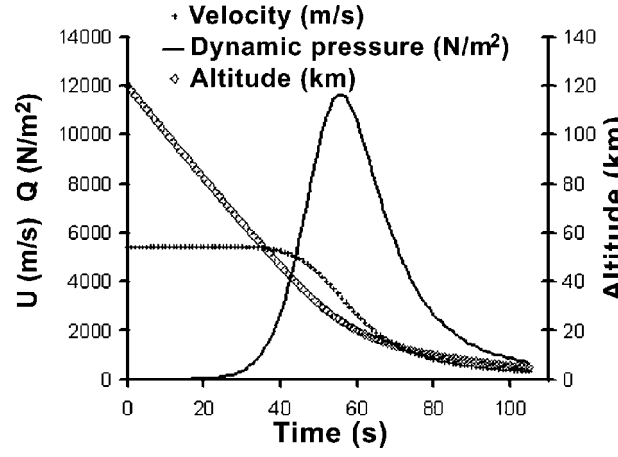

Fig. 3 Trajectory profile based on a nominal entry flight-path angle of −18 deg.

were used for their superior convergence and accuracy. All computations were performed as full Navier–Stokes simulations, under the assumption of laminar flow. Transition to turbulence may occur in the wake recompression region for certain trajectory conditions, but no current turbulence model is capable of predicting this effect accurately.

Roe's flux difference upwind scheme was used. The Van Leer flux limiter was used to provide higher-order spatial accuracy. The flow was specified as a mixture of thermally perfect gases, with the specific heats and enthalpy of each species of the mixture determined as a function of temperature from a molecular database.

Fixed supersonic inflow boundary conditions were specified at the upstream grid boundaries. Extrapolation was applied at outflow boundaries. Symmetry boundary conditions were imposed at the plane of symmetry. Constant-temperature, noncatalytic wall boundary conditions were imposed at the vehicle surface. Table 3 lists the wall temperatures applied at the various trajectory points.

Chemical Reaction Set

The computational model of the Martian atmosphere employed in all analyses assumes a mixture of 97% CO_2 and 3% N_2, by mass fraction. Other trace species found in the Mars atmosphere (such as

Table 3 CFD model conditions

M	ρ, kg/m^3	Forebody wall temperature, K	Base wall temperature, K
26.45	4.647e−5	1500	300
23.89	2.712e−4	2000	300
19.36	8.208e−4	2000	300
14.60	1.615e−3	2000	300
9.76	2.767e−3	2000	300
6.85	3.803e−3	1000	300
4.90	4.818e−3	500	300
2.95	6.564e−3	300	300
1.485	9.908e−3	250	250

Ar, O_2, and CO) were not considered. This CO_2–N_2 composition has been used in previous Mars entry vehicle CFD analyses.

Park et al.[4] have compiled kinetic models suitable for Martian atmosphere entry. An eight species model is used (CO_2, CO, N_2, O_2, NO, C, N, and O) for CO_2–N_2 Mars atmosphere entry calculations. Ionization effects are not of any importance at the Mars entry velocity regime with a maximum value of 6 km/s. Ablation products are not modeled. Aerodynamic predictions with this model have shown excellent agreement with Mars Pathfinder flight data.[5] This model was used for all chemically reacting calculations. Backward reaction rates were determined from equilibrium.

Above Mach 7, chemical reactions take place, and the eight-species, nine-reaction finite rate chemistry model was employed. For Mach numbers below Mach 7, nonreacting analyses were performed for a thermally perfect gas mixture with a fixed mixture ratio of CO_2–N_2, accounting for the temperature dependence of species specific heats. Both reacting and nonreacting analyses were performed at the Mach 7 conditions to ensure consistency and smooth transition from nonreacting to reacting analyses.

Table 3 shows the freestream Mach number and density calculated from the CFD model based on the velocity, temperature, and pressure input from Table 1. The resulting Mach numbers are slightly lower than the nominal Mach numbers listed in Table 1, which are based on the more detailed Mars-GRAM atmosphere model.

Aerodynamic Force and Moment Calculation

Combined aerodynamic forces resulting from pressure and viscous forces acting on the vehicle walls were computed internally by the CFD-FASTRAN code. Aerodynamic coefficients presented throughout this report are nondimensionalized with the freestream dynamic pressure, $Q = 1/2\rho U^2$. The vehicle diameter, $D = 0.9$ m, was chosen as the reference length, and the projected frontal area, $A = 0.6362$ m^2, was used as the reference area. The reference location for the moment coefficient was the nose of the vehicle.

Computational Grid

CFDRC's CFD-GEOM[6] grid generation software was used to generate all computational grids for this project. The computational grid was designed with optimization for an aerodynamic force analysis in mind. A near wall grid spacing with a $y+$ value on the order of 1.0–5.0 was deemed acceptable for adequately resolving any separated flow and viscous layer effects important for force predictions. Heat transfer analysis was not the objective of this project and would have required a denser near wall grid with a minimal resolution corresponding to $y+$ of less than 1.0. Because the vehicle was specified as a body of revolution, only a 180-deg half-body grid model was constructed, under the assumption of flowfield symmetry with respect to the center plane.

A typical grid features 49 grid points between the vehicle surface and the freestream boundary, and 37 points in the circumferential direction (5-deg increments). Grid distribution varies along the surface to resolve important features, particularly in the shoulder area and the near wake flowfield. Grid singularities in the vehicle stagnation region and the base region were avoided by locally using H-type grids.

The shape and standoff distance of the outer boundaries and the grid spacing near the surface were adjusted for each trajectory point,

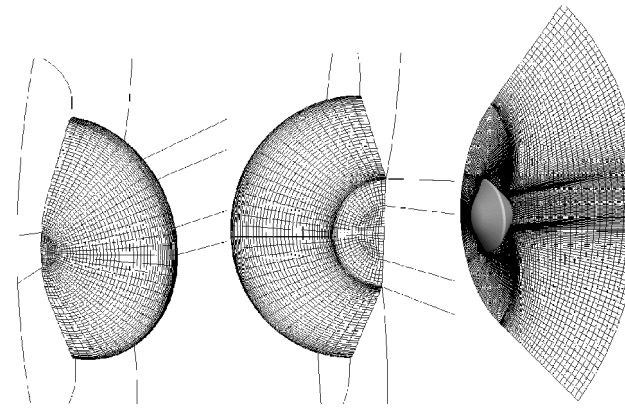

Fig. 4 Example of computational grid in plane of symmetry and on body.

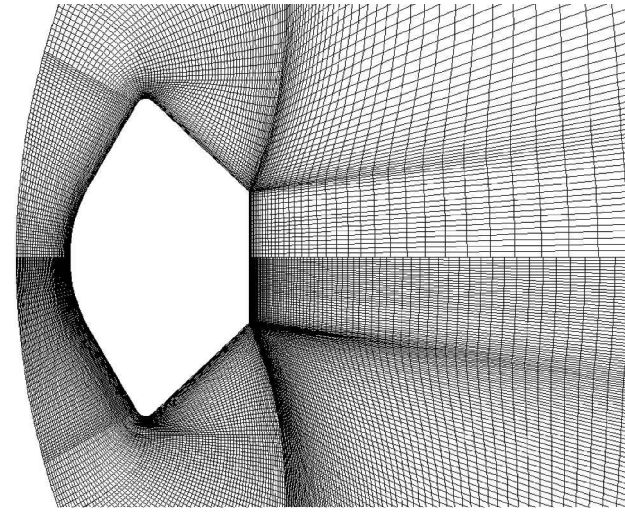

Fig. 5 Computational grids for Mach 3 grid-independent solution study.

to ensure the capture of the bow shock, the capture of the subsonic wake and the recompression region, and satisfaction of the near wall $y+$ criterion. Figure 4 shows an example of the grid distribution in the plane of symmetry and on the vehicle surface.

The total number of grid points for each case is approximately 305,000 (for a total of 275,000 grid cells) divided into nine zones. Grid size was increased for the Mach 1.5 analyses in the body-normal direction to accommodate the larger shock standoff distance and the larger enclosed angle of the trailing shock surface. The grid was extended in the axial direction because the subsonic wake extends significantly farther downstream compared to supersonic and hypersonic wakes. At Mach 1.5, the computational grid consisted of 507,000 grid points and 464,000 cells in five zones.

Grid-Independent Solution Study

An axisymmetric grid refinement study was undertaken to determine the requirements for a grid-independent solution. The equally distributed circumferential grid experiences much smaller gradients and is sufficiently resolved. Cases were run at Mach 3 without chemical reactions, and at Mach 20 with finite rate chemistry effects. Two axisymmetric grid models were analyzed, a baseline grid and grid doubled in both directions (along the body surface and normal to it). Figure 5 shows a comparison of the baseline and refined grid for the Mach 3 case.

To ascertain the grid dependence in the circumferential direction, a three-dimensional baseline grid model was analyzed at $\alpha = 0$ deg and compared to the baseline grid axisymmetric solution. The results of the grid refinement study are summarized in Table 4. Good agreement was achieved for both reacting and nonreacting analyses

Table 4 Grid dependence study

Grid density	C_A
Mach 3, nonreacting	
Axisymmetric, baseline grid	1.5094
Axisymmetric, refined grid	1.5095
Three-dimensional, baseline grid, $\alpha = 0$ deg	1.5085
Mach 20, reacting	
Axisymmetric, baseline grid	1.4598
Axisymmetric, refined grid	1.4600
Three-dimensional, baseline grid, $\alpha = 0$ deg	1.4596

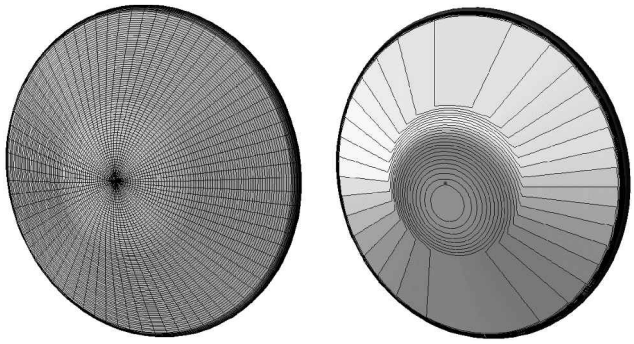

Fig. 6 Modified Newtonian flow: surface model and pressure distribution ($\alpha = 8$ deg).

with differences on the order of a fraction of a percent and well below the overall computational uncertainty.

Newtonian Theory Aerodynamics

A small computer program was written specifically for the Beagle 2 geometry, to compute the aerodynamic coefficients predicted by the modified Newtonian flow theory. The local surface pressure coefficient is computed with the modified Newtonian sine-squared law:

$$C_p = C_{p\max} \sin^2 \theta \tag{1}$$

The angle θ is the angle between the freestream velocity vector and the local surface tangent. $C_{p\max}$ is the maximum pressure coefficient, evaluated at a stagnation point behind a normal shock using the Rayleigh pitot tube formula for frozen gas chemistry (constant γ). In the limit $M \to \infty$ the maximum pressure coefficient becomes

$$C_{p\max} = [(\gamma + 1)^2/4\gamma]^{\gamma/(\gamma-1)}[4/(\gamma + 1)] \tag{2}$$

The surface definition accounted for the Beagle 2 forebody and shoulder. The backshell was not modeled, for which the pressure coefficient is zero in the so-called shadow region of the forebody. The surface was discretized into small surface panels, and the modified Newtonian value was determined locally to predict the force increments for each panel. The overall force and moment coefficients were then obtained as the summation over all panels.

Figure 6 shows the surface discretization used, along with an example of the resulting pressure coefficient distribution for $\alpha = 8$ deg. These coefficients were included in Fig. 6 plots of the CFD predictions for aerodynamic coefficients.

Results

Computed Aerodynamic Coefficients

Computed axial force, normal force, and pitch moment coefficients are plotted as functions of the Mach number in Figs. 7–9, respectively, whereas Figs. 10–12 present the data as functions of angle of attack. Aerodynamic coefficients predicted by the modified Newtonian law are included in the plots of Figs. 7–12 as a reference. A value of $\gamma = 1.15$ was used in computing the value for $C_{p\max}$. This γ value is a typical average of hypersonic postshock effective γ levels predicted for reacting flow Martian entry.[7]

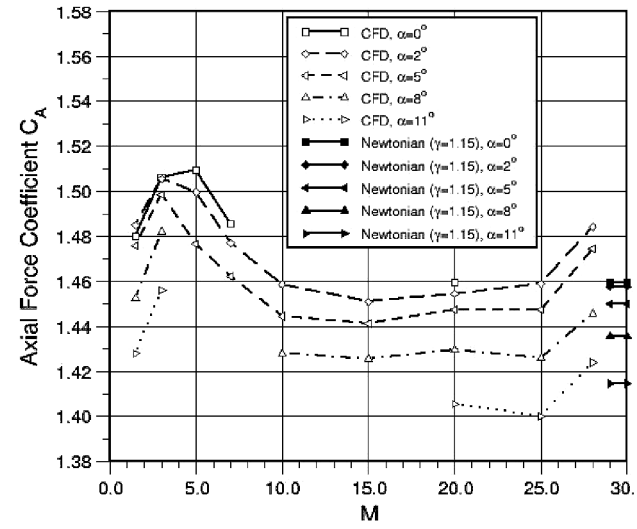

Fig. 7 Axial force coefficients as a function of Mach number.

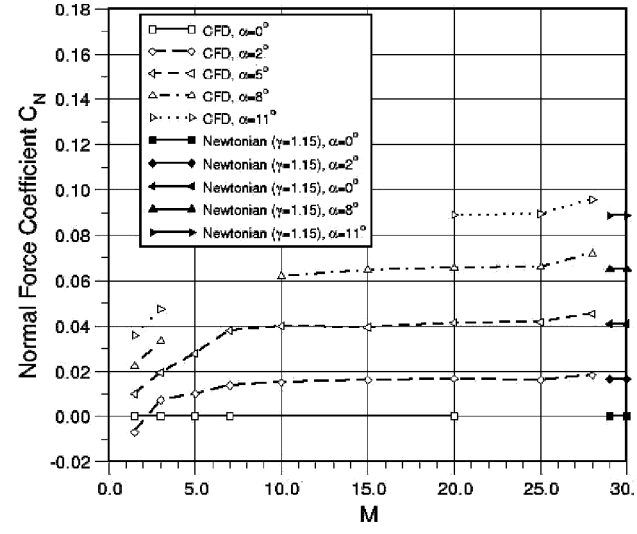

Fig. 8 Normal force coefficients as a function of Mach number.

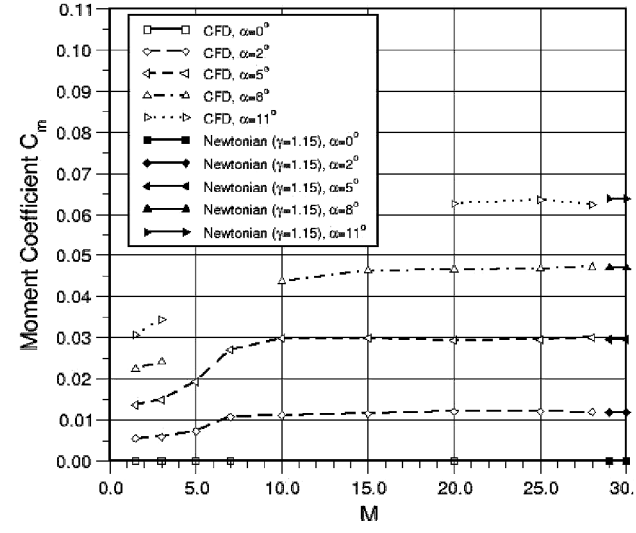

Fig. 9 Moment coefficients as a function of Mach number.

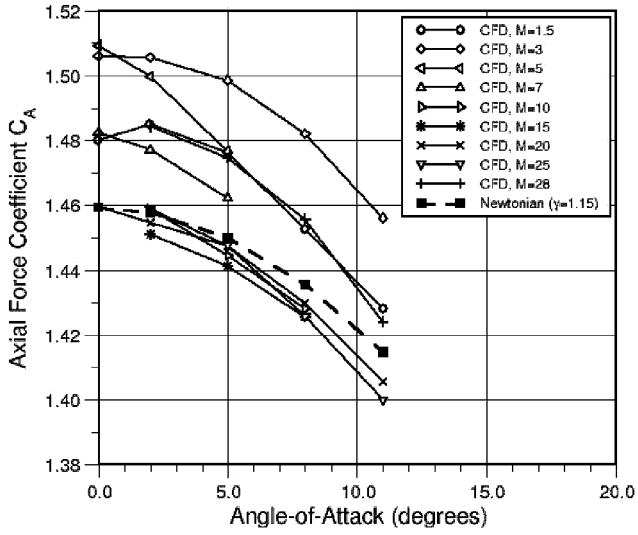

Fig. 10 Axial force coefficients as a function of angle of attack.

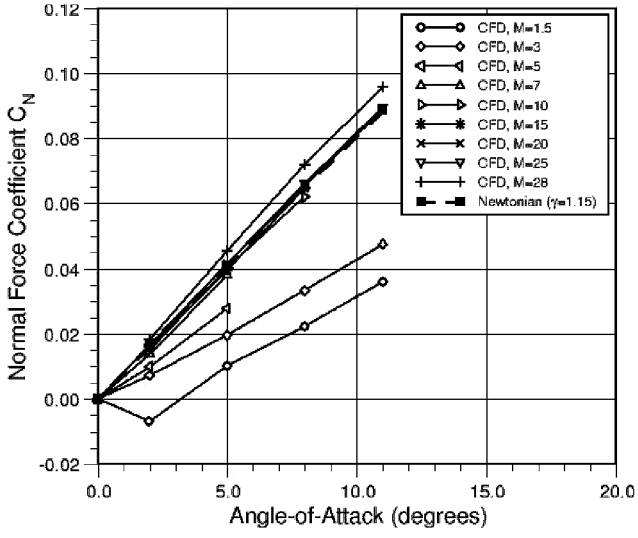

Fig. 11 Normal force coefficients as a function of angle of attack.

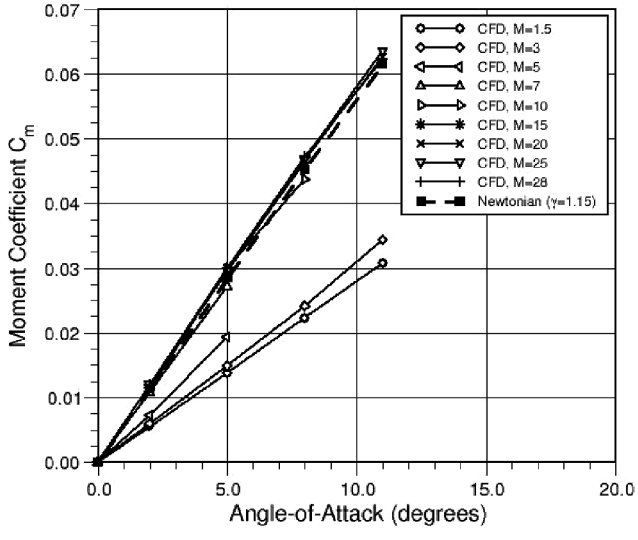

Fig. 12 Moment coefficients as a function of angle of attack.

Note from Figs. 7–12 that the Newtonian flow assumption is quite good for Mach numbers above 10. Flow at $M = 28$ is transitional, with a Knudsen number of approximately $Kn = 0.005$, on the edge of continuum flow, which is typically defined at $Kn = 0.001$. The rise evident in aerodynamic coefficients for this regime is consistent with the transition to rarefied flow.

Axial force values predicted from Newtonian flow agree reasonably well with the CFD results (Fig. 7). Newtonian flow normal force and moment coefficients agree very well with CFD results for $\alpha < 5$ deg and only slightly underpredict for $\alpha > 5$ deg. Transition from the Newtonian level to the half-Newtonian level occurs for the normal force and moment coefficients below Mach 10, whereas the axial force coefficient rises sharply.

The transition from a Newtonian to half-Newtonian force magnitude is closely related to the shift of the sonic line in the shock layer as a function of the gas chemistry. Figure 13 shows the location of the bow shock and the sonic line in the plane of symmetry at various Mach numbers for $\alpha = 5$ deg. Figure 14 shows the corresponding surface pressure distribution along the plane of symmetry.

At Mach 3, the pressure distribution is well rounded, which is typical for a subsonic shock layer. The sonic line is located on the edge of the conical forebody near the cone–shoulder junction for the lower Mach numbers. A subsonic region encloses the complete forebody, resulting in a smooth rounded pressure distribution.

For the higher Mach numbers, the sonic line outside the boundary layer moves forward toward the junction of the cone and spherical nose. The pressure distribution over the conical forebody is nearly flat in the region of the supersonic inviscid portion of the shock layer (Fig. 14).

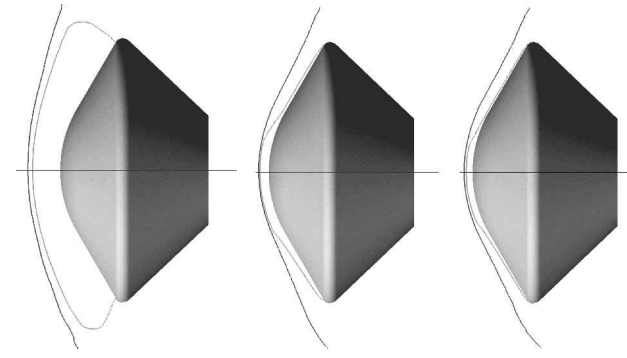

Fig. 13 Position of bow shock and sonic line at $\alpha = 5$ deg, for $M =$ a) 3, b) 10, and c) 28.

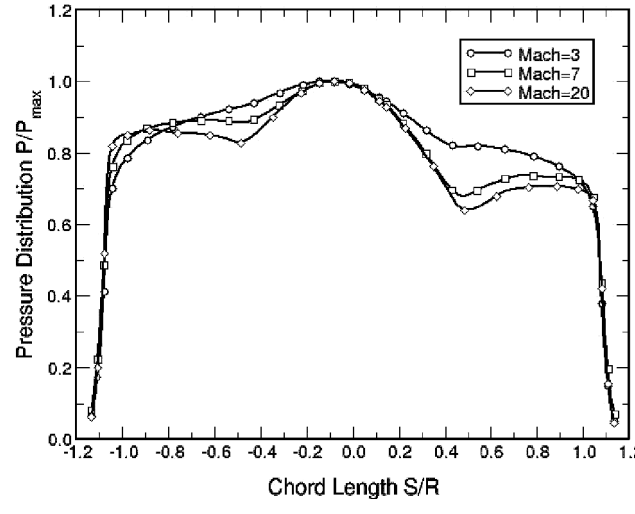

Fig. 14 Surface pressure distribution in plane of symmetry for $\alpha = 5$ deg.

Unsteady Nature of Flow at Mach 1.5

At Mach 1.5, the transonic flow cases presented the greatest difficulty when attempts were made to obtain a converged flowfield and to determine the aerodynamic characteristics. It was concluded that a steady-state solution could not be achieved due to the unsteady nature of the base flow. Evaluation of numerous two- and three-dimensional computational models with varying levels of time accuracy and grid resolution confirmed that the time-varying forces are due to the interaction of the base flow shock and the shear layer shedding over the vehicle frustrum. Forces computed on the front shield of the vehicle are absolutely steady, whereas those on the frustrum and the base are time variant due to a pulsating motion of the shock in the base region and the shear layer over the vehicle frustrum. In three-dimensional flow, the initially axisymmetric toroidal vortices shed over the frustrum are inherently unstable and are easily perturbed to dissipate and become three-dimensional, nonaxisymmetric vortical structures.

Time-dependent, three-dimensional computations of axial force initially enter a pulsating pattern consistent with two-dimensional results, with the normal force and moment coefficients being zero. After a number of time steps, the axially symmetric shear-layer vortices are perturbed and turn to almost random, three-dimensional vortical structures. Normal force and moment coefficients quickly develop nonzero, seemingly random oscillations, and the axial force coefficient also deviates from the initially periodic pulsation to a somewhat random fluctuation.

The flowfield is most sensitive at small angles of attack. In fact, there is great difficulty in the determination of a distinct difference in coefficients between 0- and 2-deg angles of attack. An effective angle of attack induced by the unsteady base flow is at least on the order of 2 deg. The mean oscillation levels are easier to distinguish for the larger angles. Time accurate simulations were performed for the Mach 1.5 condition, and the mean and lower/upper bounds of the fluctuating aerodynamic coefficients were extracted.

Wake Evolution

Shown in Fig. 15 are contours of absolute velocity for four Mach numbers (3, 10, 20, and 28), all at $\alpha = 5$ deg. The Fig. 15 plots show the shape and extent of the wake as it changes over the Mach number range, as well as the movement of the separation point on the back cover.

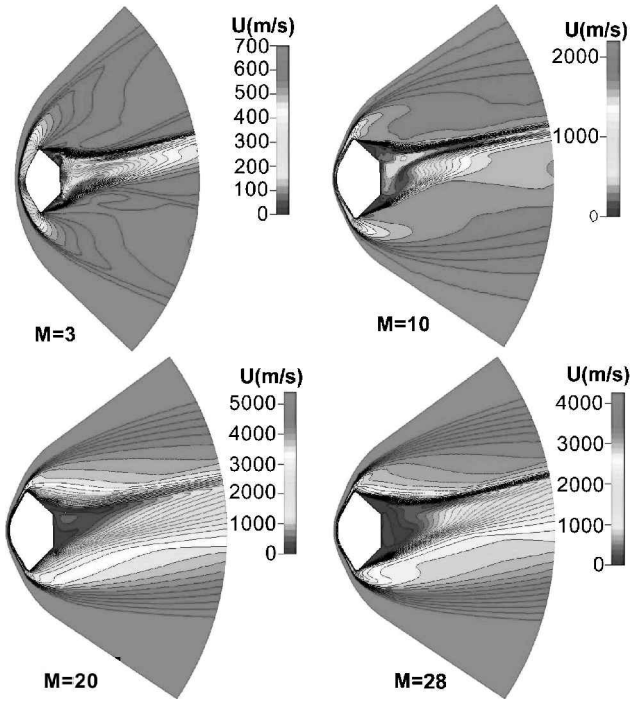

Fig. 15 Evolution of the wake ($\alpha = 5$ deg); contours of absolute velocity (m/s).

Attached flow remains evident for a portion of the conical back cover at the high Mach numbers. At these high Mach numbers, the wake is narrow. As we move down in Mach number, the flow separates farther upstream until it separates even upstream of the maximum diameter point on the shoulder for the lower Mach number. The wake widens and results in supersonic reverse flow toward the base.

Localized Geometry Features

During the derivation of the static aerodynamic database, a number of geometry changes occurred to the vehicle. Most notable are the presence of the launch clamp ring in the base and the 5-mm rear-facing step just downstream of the maximum diameter of the probe. The rear-facing step was necessary to allow for exacting manufacturing tolerances and to help promote separation over the entire aft cover. The launch clamp ring is required to allow for mounting to the Mars Express mother ship.

One additional case that was analyzed evaluated the effect of an asymmetric backward step at $\alpha = 0$ deg. The base portion of the grid was moved vertically by a small amount (2 mm) to generate a 7-mm-high step at the top and a 3-mm step at the bottom of the configuration. This level of asymmetry is an extreme within the prescribed vehicle manufacturing tolerances.

Table 5 summarizes the differences in the aerodynamic coefficients due to the presence of the rear-facing step and the launch clamp ring for the $M = 7$ condition at $\alpha = 0$, 2, and 5 deg. There is a slight increase of the axial force coefficient due to the addition of the step and the launch clamp ring. The effect on the normal force and moment coefficients is inconclusive. The asymmetry in the base results in only minute normal force and moments on the order of 10 drag counts or fewer. This is within the accuracy limit of the force computation.

A comparison of the velocity field and the temperature field around the two configurations is shown in Figs. 16 and 17. The strong reverse wake flow toward the base is altered by the launch clamp ring. The base flow shock standoff distance is increased, and the flow is not attached to the outer portion of the base. The temperature field shows a reduction in the peak temperatures near the base as the hot gases are diverted from the outer edge of the base.

Table 5 Variation in aerodynamic coefficients due to geometry variations at Mach 7

α, deg	C_A	C_N	C_m
	Original		
0	1.4820	0	0
2	1.4770	0.0138	0.0108
5	1.4622	0.0380	0.0271
	Modified, symmetric		
0	1.4860	0	0
2	1.4832	0.0154	0.0110
5	1.4712	0.0375	0.0259
	Modified, asymmetric		
0	1.4820	−0.0007	0.0001

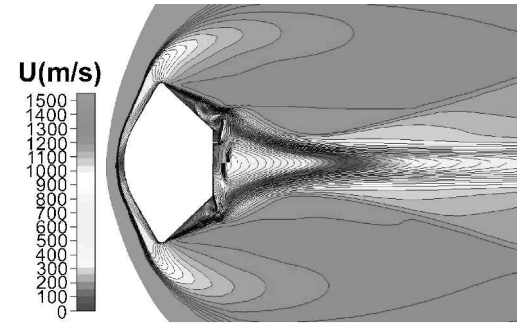

Fig. 16 Contours of absolute velocity (m/s) at $M = 7$: top, with back step and launch clamp ring and bottom, without back step and launch clamp ring.

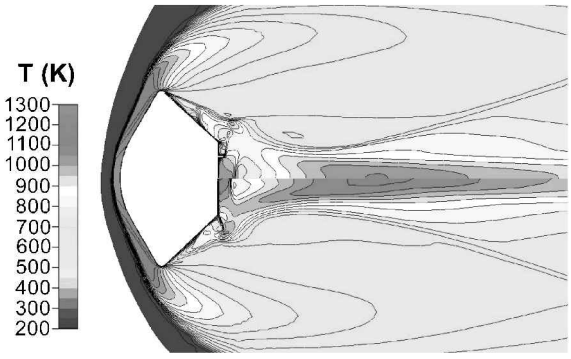

Fig. 17 Temperature contours (K) at Mach 7: top, with back step and launch clamp ring and bottom, without back step and launch clamp ring.

Blended Aerodynamic Database

The aerodynamic data presented in this paper were used in the construction of a blended database for the Beagle 2. Derivation and details of the blended Beagle 2 database are presented in Ref. 8 and are not repeated here. Data sets employed in the blending process comprise the Beagle 2 CFD data presented here, data obtained for the A2 phase of the Huygens development and scaled to suit the Beagle 2, wind-tunnel data for the Huygens probe, wind tunnel and CFD data for the Stardust sample return capsule,[9] data obtained for the Mars Pathfinder,[5] and data scaled from NASA experimental results obtained for a 60-deg cone.[10] The blended database covers a total angle of attack range of 0–30 deg and a Mach range of 0.4–28.

Conclusions

CFD analyses were performed for more than 50 cases to generate an aerodynamic database applicable over the Beagle 2 entry trajectory regime. Newtonian approximations hold very well for Mach numbers above 10. Below Mach 10, transition to the half-Newtonian level occurs for the normal force and moment coefficients, whereas the axial force components rise sharply. The base flow at the Mach 1.5 condition was found to be unsteady due to oscillations induced by the interaction of the separation shear layer and the strong reverse base flow. Evaluation of local effects such as the addition of a back step at the shoulder/back shield junction and the inclusion of the launch clamp ring show small effects on overall aerodynamics.

References

[1] "CFD-FASTRAN, Version 2002, User's Manual," CFD Research Corp., Huntsville, AL, March 2002.

[2] Muylaert, J., Walpot, L., Spel, M., Tumino, G., and Steijl, R., "Nonequilibrium Computational Analysis of Blunt Cone Experiments Performed in the LENS and HEG Facilities," AIAA Paper 96-2436, June 1996.

[3] Justus, C. G., James, B. F., and Johnson, D. L., "Mars Global Reference Atmospheric Model (Mars-GRAM 3.34): Programmers Guide," NASA TM-108509, May 1996.

[4] Park, C., Howe, J. T., Jaffe, R. L., and Candler, G. V., "Review of Chemical Problems of Future NASA Missions, II: Mars Entries," *Journal of Thermophysics and Heat Transfer*, Vol. 8, No. 1, 1994, pp. 9–23.

[5] Gnoffo, P. A., Braun, R. D., Weilmuenster, K. J., Mitcheltree, R. A., Engelund, W. C., and Powell, R. W., "Prediction and Validation of Mars Pathfinder Hypersonic Aerodynamic Database," *Journal of Spacecraft and Rockets*, Vol. 36, No. 3, 1999, pp. 367–373.

[6] "CFD-GEOM, Version 2002, User's Manual," CFD Research Corp., Huntsville, AL, March 2002.

[7] Gnoffo, P. A., Weilmuenster, K. J., Braun, R. D., and Cruz, C. I., "Influence of Sonic-Line Location on Mars Pathfinder Probe Aerothermodynamics," *Journal of Spacecraft and Rockets*, Vol. 33, No. 2, 1996, pp. 169–177.

[8] Burnell, S. I., Liever, P. A., and Parnaby, G., "Prediction of the Beagle 2 Static Aerodynamic Coefficients," Second Atmospheric Reentry Vehicles and Systems Symposium, Paper 111, Association Aeronautique et Astronautique de France, Les Mureaux, France, March 2001.

[9] Mitcheltree, R. A., Wilmoth, R. G., Cheatwood, F. M., Brauckmann, G. J., and Greene, F. A., "Aerodynamics of Stardust Sample Return Capsule," *Journal of Spacecraft and Rockets*, Vol. 36, No. 3, 1999, pp. 429–435.

[10] Jorgensen, L. H., and Hagen, J. R., "Measured and Computed Static Aerodynamic Characteristics of Ablating Conical Teflon Models at Mach Number 14," NASA TN D-4022, June 1967.

W. E. Williamson
Associate Editor